J. health med. sci.,
9(2):77-84, 2023.

Dose distribution for CBCT as an aid for radiation protection in dentistry

Distribución de dosis para CBCT como ayuda para la protección radiológica en odontología

Campos Méndez José Daniel[1], Arce Corrales Luis[2], Barba Ramírez Lucía[3], Noguera Vega Gerardo[1], Mora Ramírez Erick[1], Umaña Wong Alejandra[3]

Campos Méndez, J.D.; Arce Corrales, L.; Barba Ramírez, L.; Noguera Vega, G.; Mora Ramírez, E.; Umaña Wong, A. Dose distribution for CBCT as an aid for radiation protection in dentistry. *J. health med. sci., 9(2)*:77-84, 2023.

ABSTRACT: To characterize effective dose distributions in the craniofacial area for different acquisition parameters of dental cone beam CT, thermoluminescent dosimeters (TLD) were placed within an anthropomorphic phantom for measuring effective dose. Results showed higher effective doses with 8 mA compared to 3 mA. The relative high effective dose distribution was concentrated around the field of view (FOV) but extended beyond it, irradiating nearby tissues. Understanding these effective dose distributions can aid in optimizing patient safety in dental radiology practices.

KEYWORDS: Dental CBCT, anthropomorphic phantom, effective dose distribution, thermoluminescent dosimeters (TLD), craniofacial area.

INTRODUCCTION

Radiation emitters are widely used in medicine for diagnosis, but this use comes with the risk of adverse effects appearing in biological tissues. This is why the benefits must outweigh the detriments (Angelopoulos *et al.*, 2012; Ludlow & Ivanovic, 2008).

Cone beam computed tomography (CBCT) is an equipment that allows the generation of volumetric images of the human body, avoiding the limitations of two-dimensional images such as the superposition of different structures. Specifically, dental CBCT is a recent technology that has rapidly grown in dental radiology in Costa Rica where the most requested studies are for the posterior inferior part of the maxillofacial area (Barba *et al.*, 2018).

CBCT changes the common acquisition of computed tomography (CT) because the X-ray tube only needs to make one or fewer rotations to generate the volumetric image. Although the kilovoltage values are not significantly different between CT and CBCT (ranging from 80 kV to 120 kV for adults), the current value is much lower. CBCT equipment is simpler and smaller than CT, and since it is intended for dental diagnosis, patients are placed usually seated or standing (Angelopoulos *et al.*, 2012; Ludlow & Ivanovic, 2008).

Effective dose measurements have been conducted for dental CBCT machines, but the results differ among publications due to the acquisition parameters used and the machine model. For irradiations using a field of view (FOV) of 4x4 cm, the reported effective dose in the head is 22 µSv in maxillary studies. Others equipment have equivalent doses of 267 µSv, but they are under 100 µSv in the head. For the skin, the lowest value found is 17 µSv, and the highest is 189 µSv when considering effective dose (J.B. Ludlow *et al.*, 2015; J.B. Ludlow & Ivanovic, 2008; Rottke *et al.*, 2019).

Investigations report absorbed dose, equivalent dose, or effective dose values for specific organs within the craniofacial region but not the dose distributions within it. Dose distribution maps have

1 Centro de Investigación en Ciencias Atómicas Nucleares y Moleculares, CICANUM, Universidad de Costa Rica.
2 Escuela de Tecnologías en Salud, Universidad de Costa Rica.
3 Facultad de Odontología, Universidad de Costa Rica.

been created, but they use a homogeneous PMMA phantom (Rottke *et al.*, 2019). This phantom does not represent the attenuation into a human patient.

This aim of this study was to show the effective dose distributions within the craniofacial area of CBCT patients under two different combinations of acquisition parameters frequently used for irradiating an anthropomorphic phantom.

MATERIALS AND METHODS

This study was divided into three phases: first, determination of study and parameters, second, irradiations and measurement and third, plotting the effective dose distribution. First, the most frequent study and acquisition parameters used at the Faculty of Dentistry (DF) at the Universidad de Costa Rica, were identified. An anonymized database from the Radiology Department of all the CBCT exams conducted between 2018 and 2021 was analyzed. The anonymized database included: age, name of the irradiated region, FOV, current used by the X ray tube, kilovoltage used by the X ray tube, date of the acquisition. All pediatric studies were excluded due to the characteristics of the phantom, which represents an adult person. The equipment used in the Radiology Service of the DF is a CBCT dental Morita Veraviewpocs 3D R100 (Morita Corp., n.d.).

Second, after identifying the most used study, two most frequently used sets of acquisition parameters (tube current, kilovoltage, acquisition mode) were selected, thus stablishing the two protocols to be used. Additionally, the possible irradiated organs were identified using the reference list of the phantom shown by (Pauwels *et al.*, 2014) and the common anatomical ubication and FOV of the selected acquisition.

For the measurements, the head of the Alderson RANDO phantom was used (Radiology Support Devices INC, n.d.) which is an anthropomorphic phantom made of silicone and separable into slices. Each slice has different measurement points with a removable piece to be replaced by a cylindrical detector (Figure 1).

However, for the personal equivalent dose measurement, crystalline thermoluminescent dosimeter (TLD) chips were used. These TLDs were po-

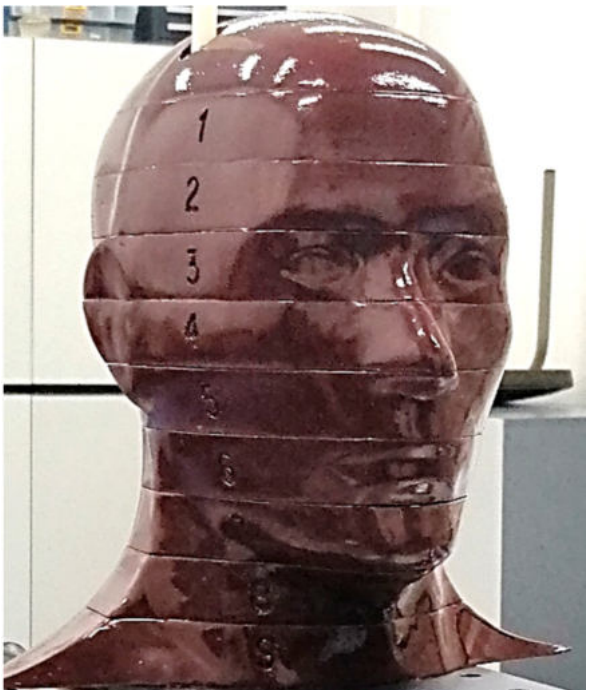

Figure 1. RANDO Alderson Phantom - Note that each slice is numbered from 1 at the top to 9 at the bottom.

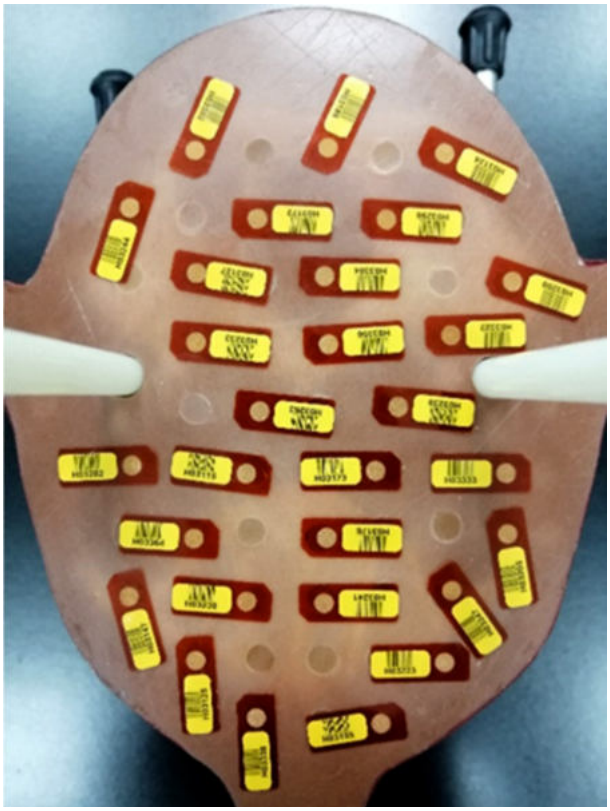
Figure 2. TLD Chip Setup on one of the slices of the RANDO Alderson Phantom.

sitioned between the slices, according to Campos & Noguera, (2023) and the same position matrix data were used to correlate the measurement with a specific point within the phantom (Figure 2).

The TLDs used for all the measurements in this research were provided by the University of Costa Rica, by the TLD laboratory at the Centro de Investigación en Ciencias Atómicas Nucleares y Moleculares (CICANUM, for its acronym in Spanish). The TLD Laboratory of this center is accredited by ISO/IEC 17025:2017, ensuring high standards of quality and trustworthiness in dosimeter readings.

Third, the phantom with the TLDs placed inside was irradiated using the previously two selected protocols, following the usual procedure with patients (Figure 3). The irradiation took into consideration the pre-scan image (scout-view or surview) and the tomographic acquisition. The TLDs were read and cleaned between irradiations.

Effective dose distribution plots were created using the ROOT Data Analysis Framework (CERN, 1996). ROOT takes the data from each point and plots the distribution by interpolating between them, resulting in a color map of a two-dimensional axial slice of the phantom. This processing was repeated for each irradiation and each slice used.

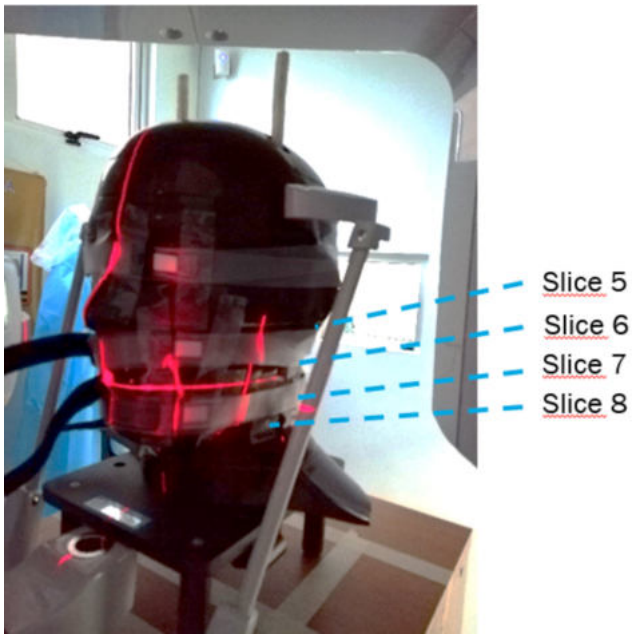

Figure 3. Phantom Positioning for each irradiation. Some TLDs are placed on the surface to measure absorbed dose in the skin and crystalline lens. The locations of the studied slices are indicated.

RESULTS AND DISCUSSIONS

Analysis of the information revealed that 440 CBCT acquisitions were made between 2018 and 2020. The number of patients could have decreased due to the COVID-19 pandemic and the restrictions imposed in the country and university. Out of these acquisitions, 52 corresponded to underage individuals and were subsequently exclude. Therefore, for the determination of the most used diagnostic study and parameters, we analyzed 388 patient irradiations. Acquisitions were not separated based on the side (left or right) due to the symmetry of the head, meaning that the effective dose distribution on one side could be reflected on the other.

The most frequently used diagnostic study was the mandibular molar, used in 123 cases, followed by the maxillary, which was used in 52 cases, then, it can be confirmed that the most requested acquisitions are the ones in the inferior posterior zone (Barba *et al.*, 2018). The most commonly used FOV was 4x4 cm. The two most frequently used sets of acquisition parameters were (90 kV, 3 mA) in 37.5% of the cases and (90 kV, 8 mA) in 28.5% of the cases.

Since the selected FOV of the selected region did not cover the entire head, TLDs were placed in the slices exposed to direct radiation as well as the slices directly above and below the FOV. According to the phantom nomenclature, these slices were 5, 6, 7, and 8. Additionally, dosimeters were placed on the skin, eyes, and in the frontal part of slice 9 (Figure 3).

After each irradiation, the dosimeters were read to obtain measurements in generic units (gU). The data obtained on the surface (skin, eyes) were reported as personal equivalent dose. However, it was not possible to do the same for the internal measurements because there are no calibration factors for different depths within the tissue for the TLD crystal used in this research.

Figure 4 illustrates the comparison between the irradiations, showing a notable difference and a non-homogeneous increase in effective dose. The greatest contrast between measurements is obser-

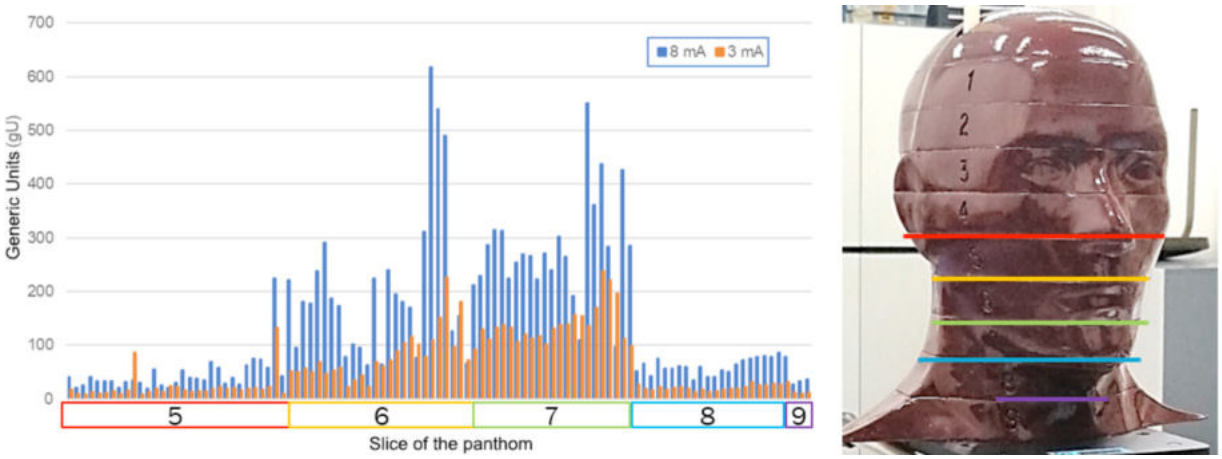

Figure 4. Comparison of measured values between irradiations. The different slices are identified by a color code corresponding to the lines on the phantom picture.

ved in the 6th slice, which corresponds to the region of the phantom containing the molars and is close to the center of the FOV. This behavior is important in the determination of the most appropriate parameters for this kind of acquisitions accompanied by the diagnostic standards.

The personal equivalent dose measured on the skin ranged between 1.6 µSv and 32.4 µSv for irradiations with 3 mA, and between 7.0 µSv and 70.7 µSv when 8 mA was used. It is important to note that these values do not represent the average personal equivalent dose on the facial skin due to the placement of superficial dosimeters at specific points on the surface of the irradiated side of the head. Determining an average skin personal equivalent dose is challenging due to the heterogeneous distribution of skin dose and the non-centered FOV in the phantom.

The measured personal equivalent doses for the crystalline lens on the right side, farthest from the FOV, were 6.5 µSv and 12.4 µSv for 3 mA and 8 mA, respectively. These values were slightly higher than the corresponding values on the left side of the phantom, which were 3.9 µSv and 11.9 µSv. Since the crystalline lens dosimeters were outside the FOV, the personal effective dose values were influenced by scattered radiation, leading to lower measurements close to the background irradiation dose. Higher values on the opposite side of the FOV positioning remains under investigation, but probably it is due to the irregular distance between the X-ray tube and the skin when the FOV is not centered on the patient, resulting in closer proximity to the skin when irradiating on the opposite side of the FOV position. The measured values in slice 9 indicate that the effective dose near the thyroid glands is close to the background effective dose under 35 gU, this is caused by the small size of the FOV and the distance between it and the thyroid glands. It is important to determine these values when a bigger FOV is used.

After processing the data, two color maps representing the effective dose distribution for each slice were generated, one for the irradiation with 3 mA and another for 8 mA. Figure 5 displays the effective dose distribution in slice 5, which is located above the FOV.

As a result, the color scale values are relatively low. The hot spots, indicating regions or points with the highest effective dose, are observed near

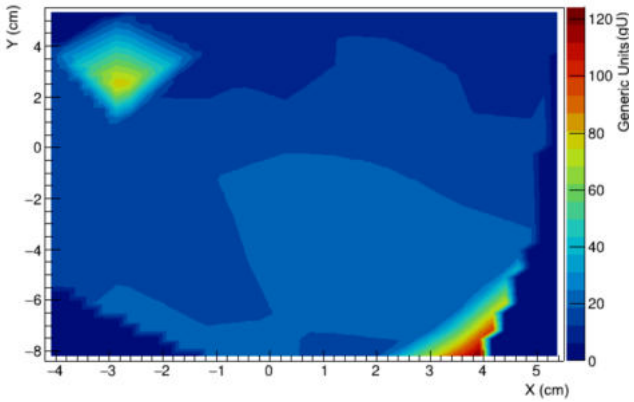

Figure 5. Color Map of Dose Distribution in Slice 5 for the irradiation using 3 mA and 90 kV. The color scale is shown on the right.

the surface in the frontal part of the phantom, just above the FOV, and at the back of the phantom in the opposite direction. This distribution pattern is consistent with the one obtained using 8 mA (Figure 6), where the hot spot at the back is less prominent but still present.

All slices exhibit a similar effective dose distribution for both irradiations. Comparing Figure 7 with Figure 8, and Figure 9 with Figure 10, it can be observed that the hot spot of the effective dose distribution shifts approximately 1 cm backward when 8 mA is used. This shift is due to the positioning of the phantom, as it was moved forward by that amount, and not due to an unexpected change in the effective dose distribution. Despite the similarity in the effective dose distribution, the measured values differ

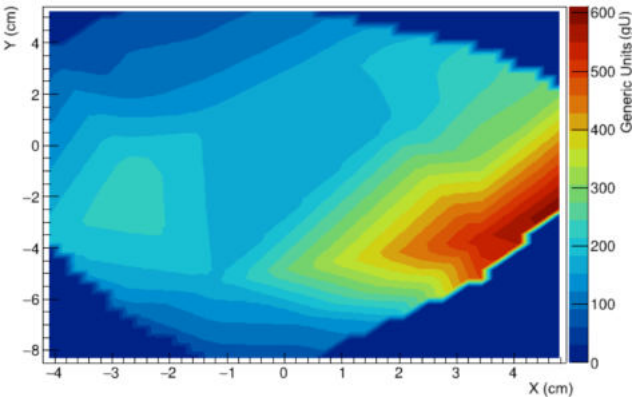

Figure 8. Color Map of Dose Distribution in Slice 6 for the irradiation using 8 mA and 90 kV. The color scale is shown on the right.

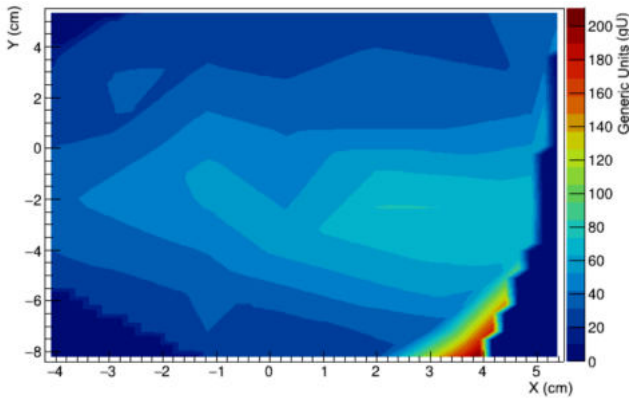

Figure 6. Color Map of Dose Distribution in Slice 5 for the irradiation using 8 mA and 90 kV. The color scale is shown on the right.

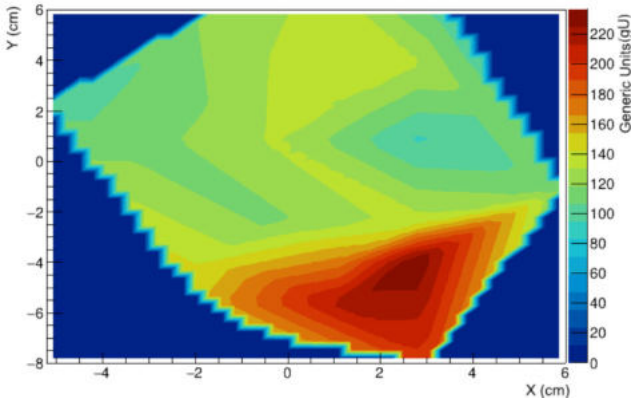

Figure 9. Color Map of Dose Distribution in Slice 7 for the irradiation using 3 mA and 90 kV. The color scale is shown on the right.

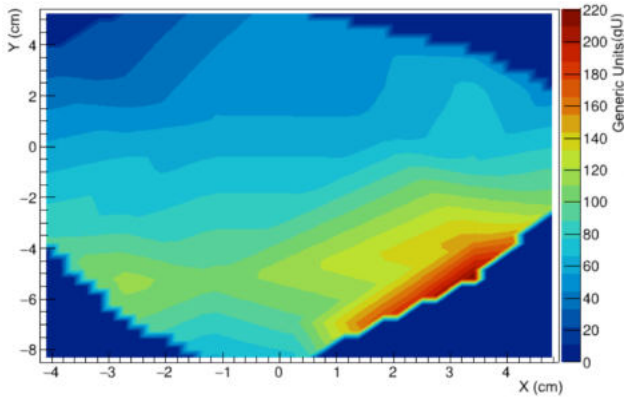

Figure 7. Color Map of Dose Distribution in Slice 6 for the irradiation using 3 mA and 90 kV. The color scale is shown on the right.

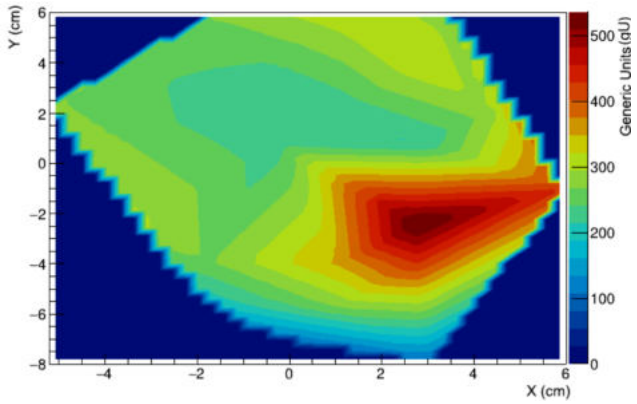

Figure 10. Color Map of Dose Distribution in Slice 7 for the irradiation using 8 mA and 90 kV. The color scale is shown on the right.

significantly. The higher values (hot spots) obtained with 8 mA are more than double those obtained with 3 mA. Then, an increase in the tube current does not change a lot the effective dose distribution into and around the FOV but increase greatly the effective dose in the tissues.

Slice 7 is entirely within the FOV (Figure 9 and Figure 10), resulting in closed isodose curves (lines with the same effective dose values). The hottest spot appears to be near the center of the FOV. However, it is important to note that the selected FOV of 4x4 cm has a cylindrical shape, while the irradiated shape resembles a triangular prism, causing relatively high effective dose values to cover a volume larger than the chosen FOV. Therefore, tissues that are not into the FOV are being irradiated with relatively high effective doses, the shape of the irradiated FOV seems to be different to the one showed on the acquired image.

Figure 11 and Figure 12 display regions of high effective doses that cover a significant area of the slice. However, it's important to consider that the dose scale used in these figures is much lower than in the others. The relatively high effective dose values at depth can be attributed to the fact that slice 8 contains less bone tissue as it is located beneath the mandibular bone.

Due to the interpolation performed, the border of the phantom appears to have a high effective dose gradient. However, this does not reflect the actual behavior of the effective dose distribution on the surface. It is caused by the absence of data outside the phantom, and the computer assumes this absence as 0 gU, resulting in the gradient serving as a bridge between high effective dose values and null effectivedose values.

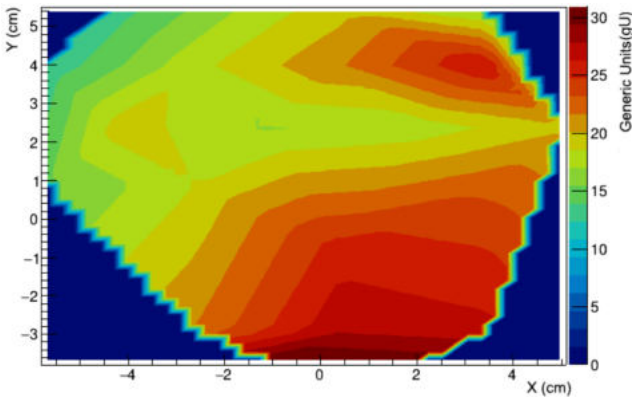

Figure 11. Color Map of Dose Distribution in Slice 8 for the irradiation using 3 mA and 90 kV. The color scale is shown on the right.

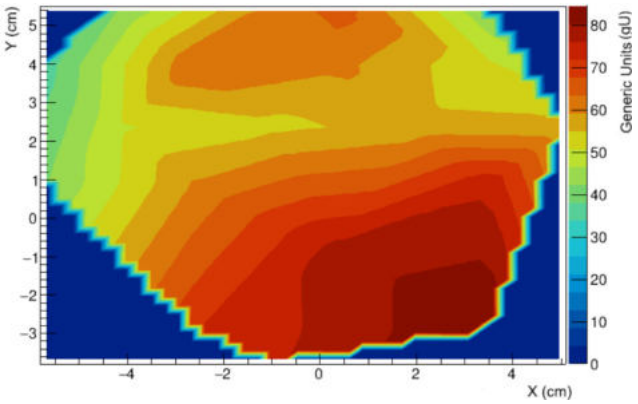

Figure 12. Color Map of Dose Distribution in Slice 8 for the irradiation using 8 mA and 90 kV. The color scale is shown on the right.

To demonstrate the effective dose distribution within the anatomical structures of the phantom, an overlapping of the color maps on a corresponding CT image occurred. The CT images was acquired in the PET/CT (Siemens Biograph Vision 450 Edge) Laboratory of CICANUM (Figure 13 and Figure 14). It is important to center the attention to the slices 6 and 7, especially in the irradiation with 8 mA, because relative high effective dose values are in the location of the parotid glands and into the oral cavity. The triangular prism shape of the irradiated FOV extends the hot spot to tissues that are part of the images and that are relatively far from the molars (the ones located on the vertex of the triangle).

In these images, the blue background was removed to show that the isodose curves do not reach the entire surface because personal equivalent dose values were measured only at specific points on the skin. RANDO phantom does not have measuring points throughout the entire area of the slices, which explains why some parts of the CT slices are not covered by the corresponding color maps, as there is no information regarding the personal equivalent dose in those areas.

CONCLUSIONS

It was determined the effective dose distribution in an average adult patient during a dental CBCT irradiation using two different sets of acquisition para-

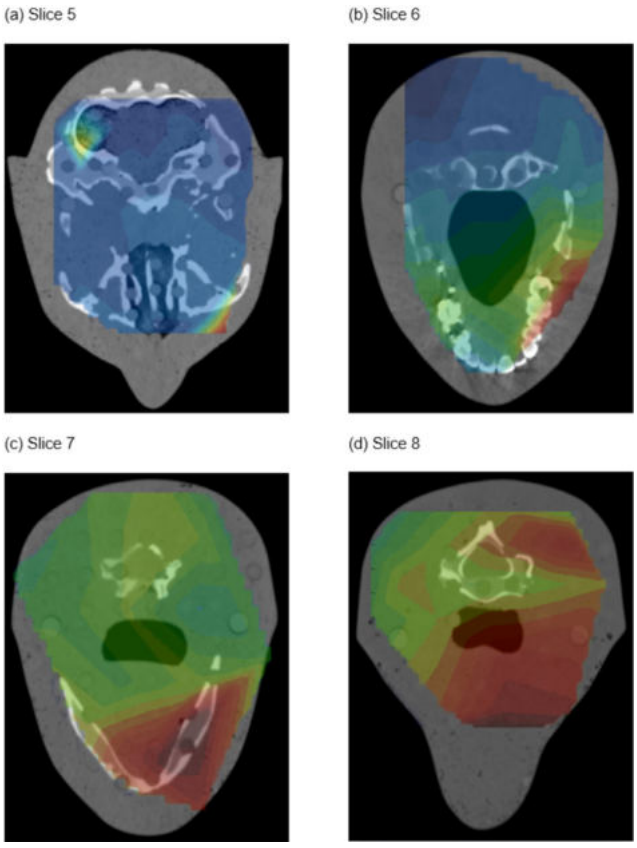

Figure 13. Superposition of Color Maps for the irradiation using 3 mA and 90 kV over the corresponding CT images.

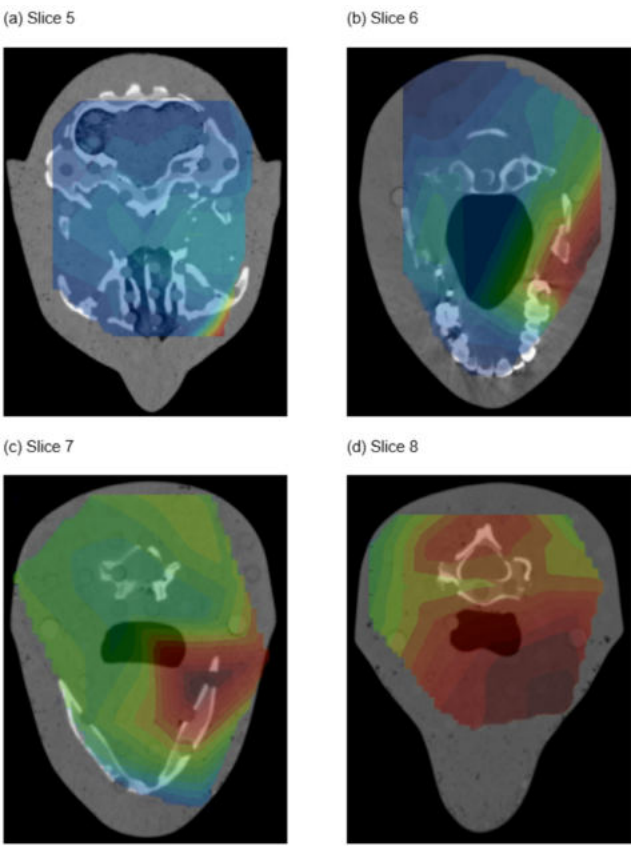

Figure 14. Superposition of Color Maps for the irradiation using 8 mA and 90 kV over the corresponding CT images.

meters, for mandibular molars. The distributions were visualized through color maps and superimpositions.

By comparing two sets of acquisition parameters, an increase in the equivalent dose when 8 mA is used compared to 3 mA was observed. However, the effective dose increase is not proportional across all dosimeters. The personal equivalent dose on the skin surface, measured at specific locations, ranged from 1.6 μSv to 70 μSv. As for the crystalline lens, the measured values were close to the background dose under 12.4 μSv.

The highest effective dose values were found around the region where the FOV was positioned. However, the volume of the region with relatively high effective dose values exceeded the size of the FOV, and its shape differed. Some tissues near the study area exhibited similar effective dose values to those shown in the acquired images. Additionally, the effective dose distribution far from the FOV appeared relatively homogeneous, with low values.

The results of this research provide a technical guide to determinate acquisition parameters for mandibular molars with low mA values, decreasing the effective dose in the patient including tissues that are not being diagnosed. Image quality research is needed as complement of these results.

RESUMEN: Para caracterizar las distribuciones de dosis efectivas en el área craneofacial para diferentes parámetros de adquisición de TC de haz cónico dental, se colocaron dosímetros termoluminiscentes (TLD) dentro de un fantasma antropomórfico para medir la dosis efectiva. Los resultados mostraron dosis efectivas más altas con 8 mA en comparación con 3 mA. La distribución de la dosis efectiva relativamente alta se concentró alrededor del campo de visión (FOV), pero se extendió más allá, irradiando los tejidos cercanos. Comprender estas distribuciones de dosis efectivas puede ayudar a optimizar la seguridad del paciente en las prácticas de radiología dental.

PALABRAS CLAVE: CBCT dental, maniquí antropomórfico, distribución de dosis efectiva, dosímetros termoluminiscentes (TLD), área craneofacial.

REFERENCES

Angelopoulos, C.; Scarfe, W.C.; Farman, A.G. A Comparison of Maxillofacial CBCT and Medical

CT. *Atlas of the Oral and Maxillofacial Surgery Clinics of North America, 20(1):*1-17, 2012 doi: 10.1016/j.cxom. 2011.12.008.

Barba, L.; Berrocal, A.L.; Hidalgo, A. Uses of cone-beam computed tomography in San José, Costa Rica. *Imaging Science in Dentistry, 48(2):*103-109, 2018. doi: 10.5624/isd.2018.48.2.103.

Campos, J.D.; Noguera, G. Dosimeter arrangement for effective dose and isodose curves determinations into craniofacial cavity. *J. Health Med. Sci., (9)*:45-49. Retrieved from http://johamsc.com/publicaciones CERN. ROOT Data Analyzer Framework. Lausanne. 1996. doi: 10.5281/zenodo.3895860.

Ludlow, J.B.; Ivanovic, M. Comparative dosimetry of dental CBCT devices and 64-slice CT for oral and maxillofacial radiology. *Oral Surgery, Oral Medicine, Oral Pathology, Oral Radiology and Endodontology, 106(1):*106-114, 2008. doi: 10.1016/j.tripleo.2008.03.018.

Ludlow, J.B.; Timothy, R.; Walker, C.; Hunter, R.; Benavides, E., Samuelson, D.B.; Scheske, M.J. Ffective dose of dental CBCT - A meta analysis of published data and additional data for nine CBCT units. *Dentomaxillofacial Radiology, 44(1),* 2015. doi: 10.1259/dmfr.20140197.

Morita Corp. Veraviewepocs 3D R100 & F40 product brochure. Kyoto: J. Moriota MFG. Corp. Retrieved from http://global.morita.com/usa/root/img/pool/pdf/product_brochures/veraviewepocs_3d-r100-f40-l-770-0714_v17.pdf.

Pauwels, R.; Zhang, G.; Theodorakou, C.; Walker, A.; Bosmans, H.; Jacobs, R.; Horner, K. Effective radiation dose and eye lens dose in dental cone beam CT: Effect of field of view and angle of rotation. *British Journal of Radiology, 87(1042)*, 2014. doi: 10.1259/bjr.20130654.

Radiology Support Devices INC. No Title. Retrieved February 12, 2020, from http://rsdphantoms.com/radiation-therapy/the-alderson-radiation-therapy-phantom/.

Rottke, D.; Dreger, J.; Sawada, K.; Honda, K.; Schulze, D. Comparison of manual and dose reduction modes of a MORITA R100 cBcT. *Dentomaxillofacial Radiology, 48*, 2019. doi: 10.1259/dmfr.20180009.

Autor de Correspondencia
Dr. Jose Daniel Campos Méndez
Centro de Investigación en Ciencias Atómicas Nucleares y Moleculares, CICANUM, Universidad de Costa Rica.
E-mail: jose.camposmendez@ucr.ac.cr

Recibido: 15 de Enero, 2023
Aceptado: 2 de Marzo, 2023